Interaction and Multiscale Mechanics, Vol. 2, No. 4 (2009) 353-374
DOI: http://dx.doi.org/10.12989/imm.2009.2.4.353

Multiscale simulation based on kriging based finite element method

Wichain Sommanawat† and Worsak Kanok-Nukulchai‡

School of Engineering and Technology, Asian Institute of Technology, Pathumthani 12120, Thailand

(Received August 17, 2009, Accepted November 15, 2009)

Abstract. A new seamless multiscale simulation was developed for coupling the continuum model with its molecular dynamics. Kriging-based Finite Element Method (K-FEM) is employed to model the continuum base of the entire domain, while the molecular dynamics (MD) is confined in a localized domain of interest. In the coupling zone, where the MD domain overlaps the continuum model, the overall Hamiltonian is postulated by contributions from the continuum and the molecular overlays, based on a quartic spline scaling parameter. The displacement compatibility in this coupling zone is then enforced by the Lagrange multiplier technique. A multiple-time-step velocity Verlet algorithm is adopted for its time integration. The validation of the present method is reported through numerical tests of one dimensional atomic lattice. The results reveal that at the continuum/MD interface, the commonly reported spurious waves in the literature are effectively eliminated in this study. In addition, the smoothness of the transition from MD to the continuum can be significantly improved by either increasing the size of the coupling zone or expanding the nodal domain of influence associated with K-FEM.

Keywords: kriging interpolation; multiscale simulation; molecular dynamics.

1. Introduction

Over the past three decades, a new conceptual framework of material engineering has been motivated by the term "*nanotechnology*". Presently, this term deals with modeling of material behaviors at the nanometer length scale. Nanotechnology can be exploited to encompass the bottom-up process by which material properties at macro-scale level can be designed by restructuring the underlying atomistic structure. Thus, nanotechnology has the potential to realize the ideal concept of material synthesis.

To develop this new design paradigm, an understanding of material behaviors from the atomistic to the continuum scales is essential. Unfortunately, this challenge cannot be accomplished by either continuum model or molecular dynamics model alone due to its individual limitations. For instance, it was revealed that the continuum-scaled constitutive model begins to lose its effectiveness as the size of its constituencies approaches the atomistic scale. On the other hand, it is impossible to model the entire macroscopic domain with atomistic simulation even on a massive supercomputer.

† Doctoral Candidate, E-mail: st029237@ait.ac.th
‡ Professor, Corresponding author, E-mail: worsak@ait.ac.th

Thus, it is desirable to develop a special numerical model that can simulate the physical phenomena of materials over a wide range of scales of interest.

During the past decade, multiscale simulation has attracted enormous attention under these two main approaches: (1) the hierarchical multiscale simulation and (2) the concurrent multiscale simulation. In the hierarchical multiscale approach, information loss was reported in its transformation from one scale to the next. To overcome this shortcoming, the concurrent multiscale approach was then proposed. Its simulation was concurrently carried over different length scales and a coupling method was necessary to ensure seamless information transfers between them.

A numerical difficulty associated with the concurrent multiscale simulation is the false reflection of high frequency waves at the molecular/continuum interface. This problem was basically due to the discretization constraint of the continuum model. Its cutoff frequency is too low to accommodate the high-frequency waves coming from the MD model. As these high frequency waves cannot propagate into the continuum domain, they reflect back into the molecular region due to the energy conservation. Consequently, this disturbance of energy balance in the MD model affects the accuracy of the simulation.

Several efforts have been made to address the shortcoming of the concurrent multiscale methods. First among them was the Molecular Atomistic Ab initio Dynamics (MAAD) method (Abraham *et al*. 1998), in which a "hand shake" region is introduced to couple the molecular dynamics model with the continuum model. Then, the Hamiltonians of the two models are averaged for this region. In order to avoid the spurious wave reflection, the finite element (FE) mesh was graded to the fineness level of the atomistic spacing. In a related approach, Rudd and Broughton (1998) proposed the Coarse-Grained Molecular Dynamics (CGMD) method. The tight-binding in a quantum mechanics simulation method was removed from the standard MAAD and only FE and MD are coupled. In this approach, the governing equation of motion was derived from a coarse-grained energy approximation based on the exact atomic potential energy. However, by scaling down the finite element mesh, a large number of time steps must be used in CGMD.

A unified formulation of atomistic and continuum models, was later introduced by Tadmor *et al*. (1996) and referred as the Quasicontinuum (QC) method. This method links an atomistic model to the continuum model by adopting the Cauchy-Born rule. This rule assumes that the continuum energy density can be derived from the atomistic potential by introducing the deformation gradient. Then the wave reflection can be reduced by using a gradually refined mesh. However, the deformation of the atomic lattice underlying continuum points must be restricted to homogeneous deformation due to the assumption on the deformation gradient. An extended version of Cauchy-Born rule based on an exponential mapping was later proposed by Arroyo and Belytschko (2002). Their proposed method proved to be very effective in the analysis of carbon nanotube in which the curvature effect must be taken into account (Arroyo and Belytschko 2003, Arroyo and Belytschko 2004). An alternative approach for building the continuum model from the atomistic basis is the so-called the Virtual Atom Cluster (VAC) method proposed by Qian and Gondhalekar (2004). The main difference in comparison with the Cauchy-Born rule is that the VAC model is formulated without using either stress or strain update scheme. As a result, the VAC method provides the facility for direct transfer of information between the molecular and the continuum models.

In yet another approach, Belytschko and Xiao (2003) developed the bridging domain method (BDM) that addressed the coupling between the continuum model and the molecular model. The method employed the MD simulation over a localized region of interest while the continuum model was used for the rest. The two regions are allowed to overlap over the *bridging zone* where the net

Hamiltonian is taken as a linear combination of the two based on a scaling parameter. The compatibility conditions in the bridging zone can then be enforced by Lagrange multiplier techniques. Xiao and Belytschko (2004) further extended the BDM to dynamics simulation problems. Several numerical investigations were carried out to demonstrate its performance in one- and two-dimensional problems. The results confirmed its efficiency in alleviating the spurious wave reflection at the molecular/continuum interface. Zhang *et al.* (2007) further proposed the Moving Least Square (MLS) approximation to determine atomistic strain fields in the MD region as well as the bridging zone. The conservations of energy and momentum of the BDM were later proven by Xu and Belytschko (2008).

Meanwhile, Wagner and Liu (2003) proposed the bridging scale method (BSM) for the coupling between atomistic and continuum models. The molecular displacements were decomposed into the coarse and the fine scales. Unlike the BDM, BSM represents the entire domain with the continuum model while the atomistic model is only applied over a localized region. A damping kernel is used to eliminate the redundant degrees of freedom in the MD domain while keeping their effects on the reduced MD system. In much earlier time, this similar technique was implemented analytically by Adelman and Doll (1976). Park *et al.* (2005a) and Park *et al.* (2005b) further extended the BSM to two- and three-dimensional atomistic/continuum couplings respectively. However, Tang *et al.* (2006) pointed out an error source in the BSM. They then proposed a modified linear element and an exact multiscale interfacial condition to improve the accuracy of the original BSM.

In this study, a new multiscale simulation is proposed. Kriging-based finite element (K-FEM) is employed to model the continuum matrix, while the molecular dynamics (MD) is confined in a localized domain of interest. In the coupling zone, where the MD overlays the continuum model, its net Hamiltonian is postulated by the contributions from the continuum and the molecular layers based on a quartic spline scaling parameter as illustrated in Fig. 1, in comparison with the linear and non-linear scaling parameters used in the bridging model. The displacement compatibility in the coupling zone is then enforced discretely by the Lagrange multiplier technique. A multiple-time-step velocity Verlet algorithm was adopted for its time integration. The objective of this study is to investigate the effectiveness of K-FEM, with its expanded nodal domain of influence (NDOI), on the transition smoothness of the two different length scales.

This paper will first present a brief overview of K-FEM (Plengkhom and Kanok-Nukulchai 2005, Kanok-Nukulchai and Wong 2008, Wong and Kanok-Nukulchai 2009). Subsequently, the multiscale coupling method based on K-FEM and the quartic spline scaling parameter will be discussed, followed by its application to dynamic simulation of wave propagation in one-dimensional atomic lattice.

2. Kriging based Finite Element Method (K-FEM)

Kriging interpolation (Cressie 1993) was first introduced in Element Free Galerkin Method (EFGM) by Gu (2003) as a substitution for the MLS approximation because of its Kronecker delta property and its consistency. The Kriging interpolation was later applied to FEM, referred as K-FEM, by allowing the domain of influence of a node to cover more than one element layer around the node. As the Kriging interpolation is employed in this study, its brief theoretical background is presented next.

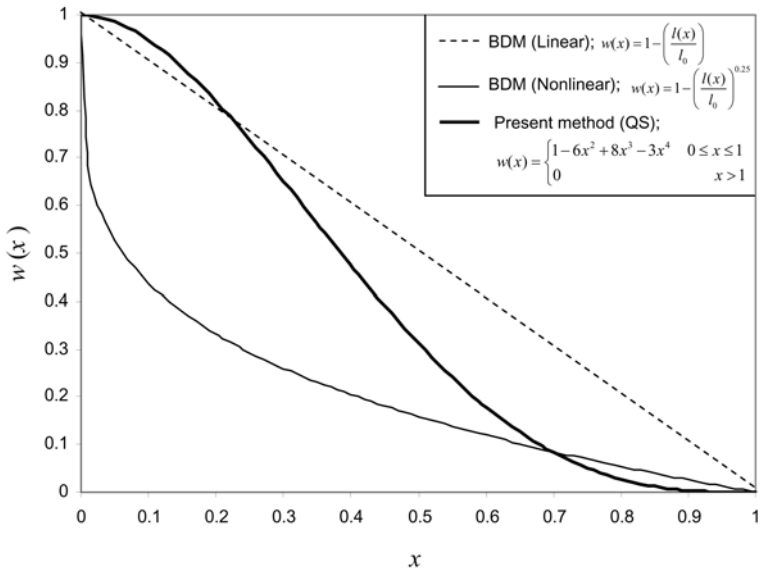

Fig. 1 Comparison of scaling parameters between the present method and the bridging domain method (Belytschko and Xiao 2003, Xiao and Belytschko 2004)

2.1 Kriging Interpolation (KI)

Consider a set of nodes denoted by $\{\mathbf{x}^a; a = 1, n\} \in \Omega_x$, where $\Omega_x \subseteq \Omega$ and n is the total number of nodes that influence a referenced location $\mathbf{x}$. The global K-FEM field, $u^h(\mathbf{x})$, can then be interpolated from $u(\mathbf{x}^a)$, *i.e.*

$$u^h(\mathbf{x}) = \sum_a^n N^a(\mathbf{x}) u(\mathbf{x}^a) \tag{1}$$

This Kriging shape function, $N^a(\mathbf{x})$, can be derived based on a polynomial basis function as follows

$$u^h(\mathbf{x}) = \sum_j^m p_j(\mathbf{x}) a_j + Z(\mathbf{x}) \tag{2}$$

where $p_j(\mathbf{x})$ is the j-term of the polynomial basis function, m is the number of terms in the polynomial basis, and $Z(\mathbf{x})$ is the departure term from the basis function with zero mean and minimized variance.

The mean square error (MSE) of the approximation field, $u^h(\mathbf{x})$, in estimating $u(\mathbf{x})$, is unbiased, *i.e.*, $E[u^h(\mathbf{x})] = E[u(\mathbf{x})]$, and can be expressed as

$$\text{MSE} = E\left[u(\mathbf{x}) - \sum_a^n N^a(\mathbf{x}) u(\mathbf{x}^a)\right]^2 \tag{3}$$

To ensure consistency, m constraints must be used to ensure that each term of the polynomial can be represented consistently by the same Kriging shape functions, *i.e.*

$$p_k(\mathbf{x}) = \sum_a^n N^a(\mathbf{x}) p_k(\mathbf{x}^a) \qquad 1 \le k \le m \tag{4}$$

Introducing the constraints of Eq. (4) with Lagrange multipliers, $\mu_k (k = 1, \ldots, m)$ into Eq. (3) leads to

$$\mathrm{MSE} = E\left[u(\mathbf{x}) - \sum_a^n N^a(\mathbf{x}) u(\mathbf{x}^a)\right]^2 + 2\sum_k^m \mu_k \left(\sum_a^n N^a(\mathbf{x}) p_k(\mathbf{x}^a) - p_k(\mathbf{x}^a)\right) \tag{5}$$

Minimizing the above equation with respect to $N^a(\mathbf{x})$ and μ_k leads to the following Kriging equation system as

$$\sum_b^n N^b(\mathbf{x}) \mathrm{cov}[u(\mathbf{x}^a) u(\mathbf{x}^b)] + \sum_k^m \mu_k p_k(\mathbf{x}^a) = \mathrm{cov}[u(\mathbf{x}^a) u(\mathbf{x})]$$

$$\sum_a^n N^a(\mathbf{x}) p_k(\mathbf{x}^a) = p_k(\mathbf{x}) \tag{6}$$

According to the intrinsic hypothesis, the covariance of the field $u(\mathbf{x})$ can be expressed as

$$\mathrm{cov}[u(\mathbf{x}^a) u(\mathbf{x}^b)] = \mathrm{cov}[\mathbf{x}^a, \mathbf{x}^b] = R(\mathbf{x}^a, \mathbf{x}^b) \tag{7}$$

where $R(\mathbf{x}^a, \mathbf{x}^b)$ is the correlation function between any pair of coupled nodes located at $\mathbf{x}^a$ and $\mathbf{x}^b$ within the subdomain Ω_x. Consequently, the Kriging equation system, Eq. (6), can be rewritten in the matrix form as

$$\begin{bmatrix} \mathbf{R} & \mathbf{P} \\ \mathbf{P}^{\mathrm{T}} & \mathbf{0} \end{bmatrix} \begin{Bmatrix} \mathbf{N}(\mathbf{x}) \\ \boldsymbol{\mu} \end{Bmatrix} = \begin{Bmatrix} \mathbf{r}(\mathbf{x}) \\ \mathbf{p}(\mathbf{x}) \end{Bmatrix} \tag{8}$$

in which

$$\mathbf{R} = \begin{bmatrix} 1 & R(\mathbf{x}^1, \mathbf{x}^2) & \cdots & R(\mathbf{x}^1, \mathbf{x}^n) \\ R(\mathbf{x}^2, \mathbf{x}^1) & 1 & \cdots & R(\mathbf{x}^2, \mathbf{x}^n) \\ \vdots & \vdots & \ddots & \vdots \\ R(\mathbf{x}^n, \mathbf{x}^1) & R(\mathbf{x}^n, \mathbf{x}^2) & \cdots & 1 \end{bmatrix}, \mathbf{R} = \begin{bmatrix} p_1(\mathbf{x}^1) & p_2(\mathbf{x}^1) & \cdots & p_m(\mathbf{x}^1) \\ p_1(\mathbf{x}^2) & p_2(\mathbf{x}^2) & \cdots & p_m(\mathbf{x}^2) \\ \vdots & \vdots & \ddots & \vdots \\ p_1(\mathbf{x}^n) & p_2(\mathbf{x}^n) & \cdots & p_m(\mathbf{x}^n) \end{bmatrix} \tag{9}$$

$$\mathbf{r}(\mathbf{x}) = \{R(\mathbf{x}^1, \mathbf{x}) \; R(\mathbf{x}^2, \mathbf{x}) \; \ldots \; R(\mathbf{x}^n, \mathbf{x})\}^{\mathrm{T}}, \mathbf{p}(\mathbf{x}) = \{p_1(\mathbf{x}) \; p_2(\mathbf{x}) \; \ldots \; p_m(\mathbf{x})\}^{\mathrm{T}} \tag{10}$$

where $\mathbf{N}(\mathbf{x}) = \{N^1(\mathbf{x}) \; N^2(\mathbf{x}) \; \ldots \; N^n(\mathbf{x})\}^{\mathrm{T}}; \boldsymbol{\mu} = \{\mu_1 \; \mu_2 \; \ldots \; \mu_m\}^{\mathrm{T}}$ $\mathbf{R}$ is the correlation matrix between pairs of nodes in the subdomain Ω_x; $\mathbf{P}$ is $n \times m$ polynomial matrix for n coupling nodes; $\mathbf{r}(\mathbf{x})$ is $n \times 1$ vector of correlations between the target point of interest, $\mathbf{x}$, and each of the influencing nodes, and $\mathbf{p}(\mathbf{x})$ is $m \times 1$ vector of the polynomial terms associated with the m basis function.

By solving the Kriging equation system, Eq. (8), the interpolant, $\mathbf{u}^h(\mathbf{x}) = \{u^h(\mathbf{x})\}$, can be expressed as follows

$$\mathbf{u}^h(\mathbf{x}) = [\mathbf{p}^{\mathrm{T}}(\mathbf{x})\mathbf{A} + \mathbf{r}^{\mathrm{T}}(\mathbf{x})\mathbf{B}]\mathbf{u}(\mathbf{x}) \tag{11}$$

in which $\mathbf{A}_{(m \times n)}$ and $\mathbf{B}_{(n \times n)}$ are defined as

$$\mathbf{A} = (\mathbf{P}^{\mathrm{T}}\mathbf{R}^{-1}\mathbf{P})^{-1}\mathbf{P}^{\mathrm{T}}\mathbf{R}^{-1}$$
$$\mathbf{B} = \mathbf{R}^{-1}(\mathbf{I}-\mathbf{P}\mathbf{A}) \tag{12}$$

where $\mathbf{I}$ is $n \times n$ identity matrix. By comparing Eq. (11) with Eq. (1), the Kriging shape function can be constructed as

$$N^a(\mathbf{x}) = \sum_j^m p_j(\mathbf{x})A_j^a + \sum_k^n r_k(\mathbf{x})B_k^a \tag{13}$$

Thus, the corresponding partial derivatives of $N^a(\mathbf{x})$ with respect to x_i can be obtained as

$$N_{,i}^a(\mathbf{x}) = \sum_j^m p_{j,i}(\mathbf{x})A_j^a + \sum_k^n r_{k,i}(\mathbf{x})B_k^a \tag{14}$$

In this study, the correlation function in Eq. (7) employs the quartic spline function, *i.e.*

$$R(\mathbf{x}^a, \mathbf{x}^b) = \begin{cases} 1-6\left(\frac{h^{ab}}{d_m}\right)^2 + 8\left(\frac{h^{ab}}{d_m}\right)^3 - 3\left(\frac{h^{ab}}{d_m}\right)^4 & \text{for } (h^{ab}/d_m) \le 1 \\ 0 & \text{for } (h^{ab}/d_m) > 1 \end{cases} \tag{15}$$

where $h^{ab} = \|\mathbf{x}^a - \mathbf{x}^b\|$ is the distance between a pair of nodes and $d_m = \max(h^{ab})$.

The typical 2D Kriging shape function and its first-order derivatives are illustrated in Fig. 2 in association with a node at $(x, y) = (2, 2)$, of which the influence covers over a domain of 4×4 identical square elements around the node. It can be observed that the Kriging shape function is a unit at the node and vanishes at all other nodes.

2.2 Layered domain of influence concept

Generally, the nodal domain of influence (NDOI) associated with a node in meshless method can be defined appropriately. Commonly used are circular and rectangular domains around the node as shown in Fig. 3. To avoid ill-condition, the number of nodes covered in each NDOI should at least equal the number of terms used in the basis function. Thus, the size of NDOI may need to vary to include sufficient number of nodes, and also to ensure that no nodes lie on the DOI boundary (Dolbow and Belytschko 1998).

Selecting the size of NDOI plays an important role in ensuring a good solution in EFGM. To maintain constructability of shape function when the nodal configuration is sparse, the size of NDOI must be varied to cover sufficient number of nodes. Furthermore, one has to be careful in ensuring that all Gauss points within the same integral cell are influenced by the same set of nodes (Dai *et al.* 2003, Kanok-Nukulchai and Plengkhom 2004). All these considerations have led to the introduction of a new concept namely the multi-layered nodal domain of influence (Kanok-Nukulchai and Plengkhom 2004, Kanok-Nukulchai *et al.* 2004). In the standard FEM, a node can only carry influence over one layer of elements around the node; consequently on the receiving end, an element can only be influenced by its own nodes. The multilayer NDOI concept allows the domain of influence of a node to propagate radially to cover more than one layer of elements around the node. Thus, an element can be influenced by its own nodes as well as *satellite nodes*,

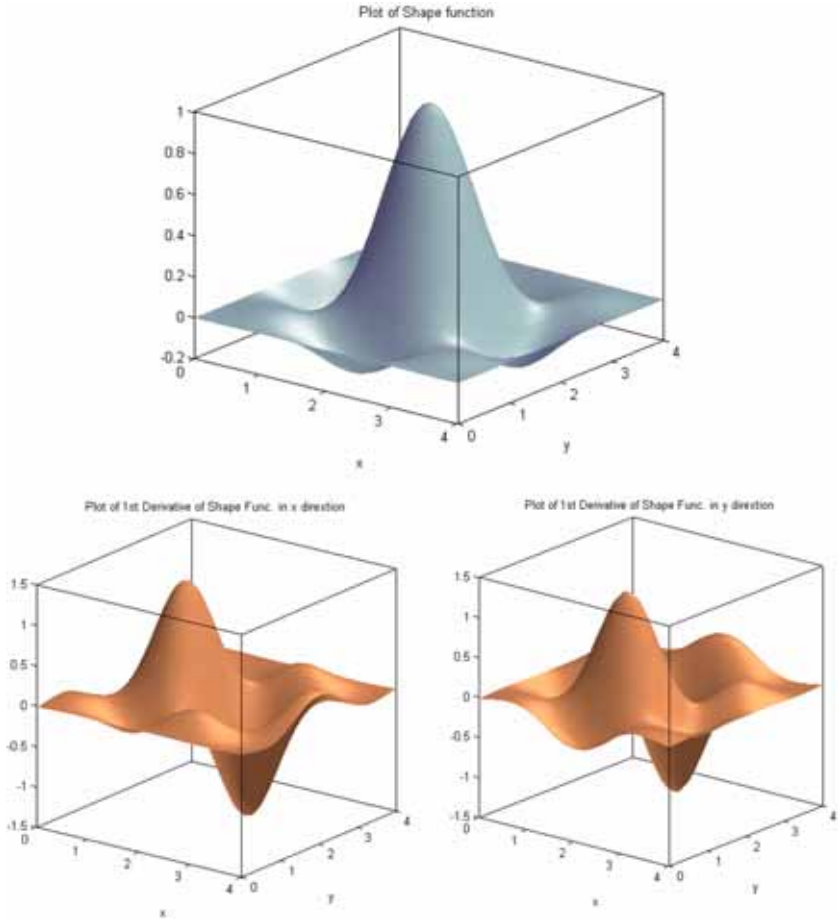

Fig. 2 Typical 2D Kriging shape function and its first order derivatives for linear basis function over 4×4 square elements around the node at (2,2)

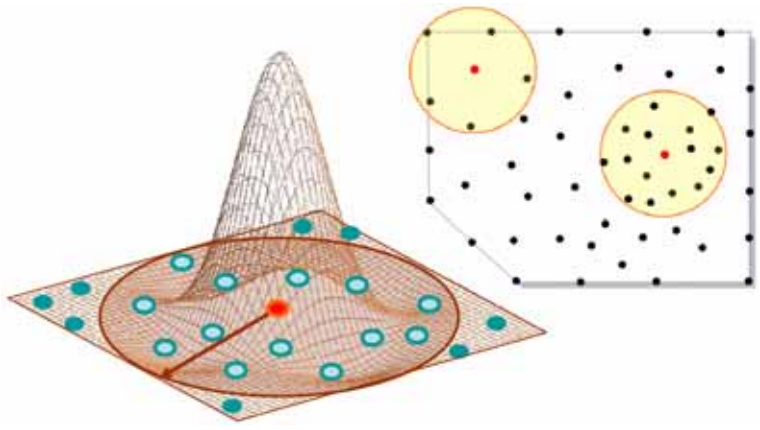

Fig. 3 Conventional domain of influence concept

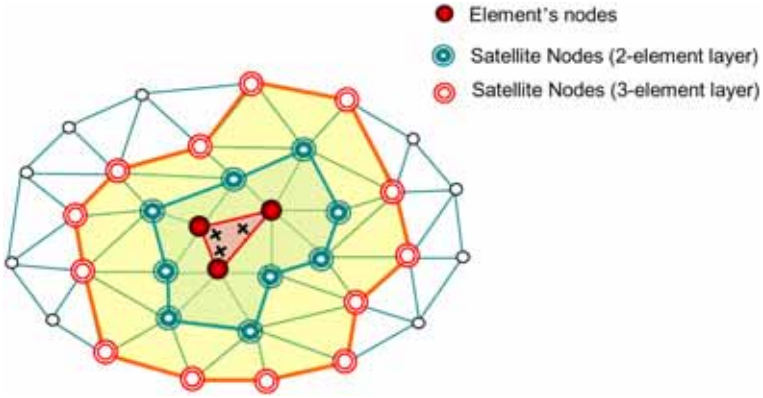

Fig. 4 Layered domain of influence concept

i.e., all influencing nodes other than its own nodes, as illustrated in Fig. 4. When one layer of elements is considered, the practice is identical to the standard FEM. It was confirmed (Plengkhom and Kanok-Nukulchai 2005) that by using the linear basis function, the results obtained from K-FEM based on one element layer of NDOI is identical to the conventional FEM. Thus, the K-FEM can be regarded as an enhancement of FEM.

3. Multiscale modeling based on K-FEM

3.1 Coupling methodology

As illustrated in Fig. 5, consider a problem domain in its initial configuration, Ω^0, composed of the following three components: (1) the continuum layer, Ω_C^0, (2) the molecular layer, Ω_M^0, and (3) the coupling zone, $\Omega_{Coup.}^0$. While the continuum layer is represented by K-FEM over the entire domain, the molecular layer is represented by an atomic model over a specific localized region where some material phenomenon is of interest. The displacement compatibility between the continuum and the molecular layers is then enforced over the coupling zones.

The total energy (Hamiltonian) in the coupling zone is determined as a summation of the continuum and the molecular energies in a proportion defined by a quartic spline scaling parameter (w). In this study, the scaling parameter varies from 1 at the $\Omega_M \setminus \Omega_{Coup.}$ interface to 0 at the $\Omega_C \setminus \Omega_{Coup.}$ interface by the following expressions

$$w(\mathbf{x}) = \begin{cases} 1 & \text{for } l(\mathbf{x}) = 0 \quad \text{at } \Omega_M \setminus \Omega_{Coup.} \\ 1 - 6\left(\frac{l(\mathbf{x})}{l_0}\right)^2 + 8\left(\frac{l(\mathbf{x})}{l_0}\right)^3 - 3\left(\frac{l(\mathbf{x})}{l_0}\right)^4 & \text{for } 0 < l(\mathbf{x}) < l_0 \text{ in } \Omega_{Coup.} \\ 0 & \text{for } l(\mathbf{x}) = l_0 \quad \text{at } \Omega_C \setminus \Omega_{Coup.} \end{cases} \tag{16}$$

where $l(\mathbf{x})$ is the orthogonal projection of $\mathbf{x}$ from $\Omega_M \setminus \Omega_{Coup.}$ and l_0 is the distance between inner and outer boundaries of the coupling zone along $l(\mathbf{x})$ projection as depicted in Fig. 6.

The Hamiltonian for the coupling zone is elucidated by a linear combination of the molecular

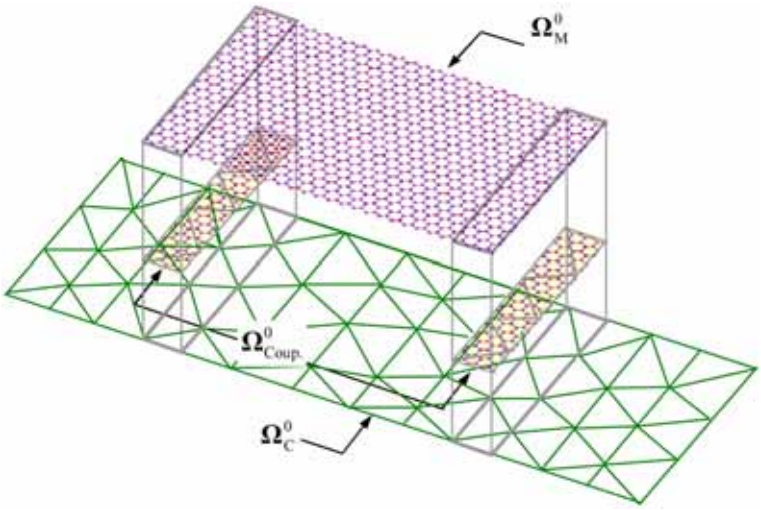

Fig. 5 Schematic illustration of layers in the present method

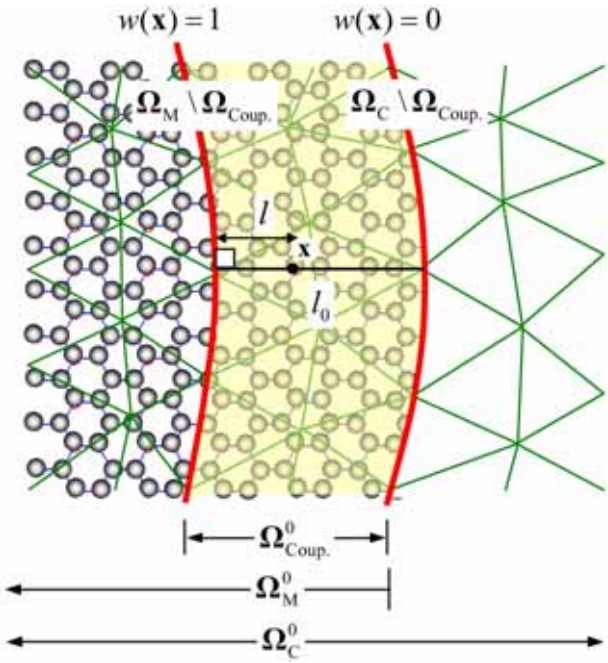

Fig. 6 Illustration of scaling parameters in coupling zone

Hamiltonian, H_M, and continuum Hamiltonian, H_C, as

$$H = w(\mathbf{x})H_M + (1 - w(\mathbf{x}))H_C \tag{17}$$

The two layers are constrained over the coupling zone, $\Omega_{Coup.}$, by

$$\mathbf{g}^a = \{g_i^a\} = \{U_i^a(\mathbf{x}^\alpha) - u_i^\alpha\} = \left\{\sum_a N^a(\mathbf{x}^\alpha)U_i^a - u_i^\alpha\right\} = 0 \tag{18}$$

where $N^a(\mathbf{x}^\alpha)$ is the shape function associated with Node a evaluated at Atom α and $i = 1,\ldots, n_{SD}$ where n_{SD} is the number of spatial dimensions. Eq. (18) states that the atomic displacements $\{u_i^\alpha\}$ are required to conform to the continuum displacements $\{U_i^a\}$ at the atomic position, α.

In the coupling zone, the Lagrangian interacting forces between the MD and the continuum layers at atomic and nodal positions respectively can be obtained as (Xiao and Belytschko 2004)

$$\mathbf{f}_\lambda^\alpha = \sum_\beta^{n_\lambda} \boldsymbol{\lambda}^\beta \frac{\partial \mathbf{g}^\beta}{\partial \mathbf{u}^\alpha} = -\sum_\beta^{n_\lambda} \boldsymbol{\lambda}^\beta \delta_{\alpha\beta} \tag{19}$$

$$\mathbf{F}_\lambda^\alpha = \sum_\beta^{n_\lambda} \boldsymbol{\lambda}^\beta \frac{\partial \mathbf{g}^\beta}{\partial \mathbf{U}^\alpha} = \sum_\beta^{n_\lambda} \boldsymbol{\lambda}^\beta N^a(\mathbf{x}^\beta) \tag{20}$$

in which $\boldsymbol{\lambda}^\beta = \{\boldsymbol{\lambda}_i^\beta\}$ is the vector of Lagrange multiplier associated with the constraints at Atom β, $\mathbf{f}_\lambda^\alpha$ and $\mathbf{F}_\lambda^\alpha$ are the Lagrangian forces at Atom α and Node a in the MD and the continuum layers respectively, while $\delta_{\alpha\beta}$ is the Kronecker delta and n_λ is the number of Lagrange multipliers.

3.2 Multiple-time-step velocity Verlet algorithm

To develop the concurrent multiscale simulation, a staggered time integration algorithm (Park and Liu 2004) was adopted for solving the coupled dynamics system with Lagrange multipliers (Xiao and Belytschko 2004). The algorithm can be described as follows.

Over one *global* time step, ΔT, the integration of the MD simulation is carried out via the velocity Verlet algorithm for a total of m micro time steps of Δt, where $m\Delta t = \Delta T$. Within each micro time step, the unknown Lagrange multipliers are determined and used in obtaining the constrained velocities for both in the continuum and the MD models. Once the MD quantities are completed for m micro time steps, the nodal quantities of the continuum model are then updated using the central differences to end the current global time step ΔT. More details of the present scheme are described in the following sections.

3.2.1 Time integration over the micro time steps

At the beginning of a typical global time station n, assuming the displacements, velocities and accelerations are already solved, the displacements of each atom for the subsequent m micro time steps can be updated using the velocity Verlet algorithm, *i.e.*

$$\mathbf{u}^\alpha_{\left(n+\frac{k+1}{m}\right)} = \mathbf{u}^\alpha_{\left(n+\frac{k}{m}\right)} + \dot{\mathbf{u}}^\alpha_{\left(n+\frac{k}{m}\right)}\Delta t + \frac{1}{2}\ddot{\mathbf{u}}^\alpha_{\left(n+\frac{k}{m}\right)}\Delta t^2 \tag{21}$$

where $0 \le k \le m-1$. Then, the acceleration of each atom can be obtained by

$$\ddot{\mathbf{u}}^\alpha_{\left(n+\frac{k+1}{m}\right)} = \frac{1}{m^\alpha}\left(\mathbf{f}^\alpha_{\text{ext}\left(n+\frac{k+1}{m}\right)} - \mathbf{f}^\alpha_{\text{int}\left(n+\frac{k+1}{m}\right)}\right) \tag{22}$$

in which m^{α} is the mass of an atom α, $\mathbf{f}_{\text{ext}}^{\alpha}$ and $\mathbf{f}_{\text{int}}^{\alpha}$ are respectively the external and the internal forces exerting on the atom α in the molecular layer.

The velocity will be obtained first at the middle of the next micro step as

$$\dot{\mathbf{u}}^{\alpha}_{\left(n+\frac{k+(1/2)}{m}\right)} = \dot{\mathbf{u}}^{\alpha}_{\left(n+\frac{k}{m}\right)} + \frac{1}{2}\ddot{\mathbf{u}}^{\alpha}_{\left(n+\frac{k}{m}\right)}\Delta t \tag{23}$$

then, the velocities for the next micro time step can then be obtained from

$$\dot{\mathbf{u}}^{\alpha}_{\left(n+\frac{k+1}{m}\right)} = \dot{\mathbf{u}}^{\alpha}_{\left(n+\frac{k+(1/2)}{m}\right)} + \frac{1}{2}\ddot{\mathbf{u}}^{\alpha}_{\left(n+\frac{k+1}{m}\right)}\Delta t \tag{24}$$

which, in view of Eq. (23), leads to

$$\dot{\mathbf{u}}^{\alpha}_{\left(n+\frac{k+1}{m}\right)} = \dot{\mathbf{u}}^{\alpha}_{\left(n+\frac{k}{m}\right)} + \frac{1}{2}\left(\ddot{\mathbf{u}}^{\alpha}_{\left(n+\frac{k}{m}\right)} + \frac{1}{2}\ddot{\mathbf{u}}^{\alpha}_{\left(n+\frac{k+1}{m}\right)}\right)\Delta t \tag{25}$$

3.2.2 Time integration over the global time steps

After completing the m micro time steps, the continuum quantities can then be updated from the global time station n to $n+1$ using the central difference method with a time step size of ΔT as follows

$$\mathbf{U}^{a}_{(n+1)} = \mathbf{U}^{a}_{(n)} + \dot{\mathbf{U}}^{a}_{(n)}\Delta t + \frac{1}{2}\ddot{\mathbf{U}}^{a}_{(n)}\Delta T^{2} \tag{26}$$

$$\ddot{\mathbf{U}}^{a}_{(n+1)} = \frac{1}{M^{a}}(\mathbf{F}^{a}_{\text{ext}(n+1)} - \mathbf{F}^{a}_{\text{int}(n+1)}) \tag{27}$$

and

$$\dot{\mathbf{U}}^{a}_{(n+1)} = \dot{\mathbf{U}}^{a}_{(n)} + \frac{1}{2}(\ddot{\mathbf{U}}^{a}_{(n)} + \ddot{\mathbf{U}}^{a}_{(n+1)})\Delta T \tag{28}$$

where M^{a} is the mass of Node a, $\mathbf{F}^{a}_{\text{ext}}$ and $\mathbf{F}^{a}_{\text{int}}$ are respectively the external and the internal forces in the continuum layer.

To determine the internal forces for continuum layer, two cases can be considered. In the region of MD overlay, the internal forces in the continuum can be obtained as

$$\mathbf{F}^{a}_{\text{int}} = \sum_{\alpha} N^{a\mathrm{T}}(\mathbf{x}^{\alpha})\mathbf{f}^{\alpha} \tag{29}$$

where $N^{a}(\mathbf{x}^{\alpha})$ is the shape function associated with Node a evaluated at the atom position $\mathbf{x}^{\alpha}$ and $\mathbf{f}^{\alpha}$ is the force acting on Atom α. This force can be obtained by differentiating the potential energy function, Φ, with respect to the corresponding position of the atom, $r_{\alpha\beta} = \left\|\mathbf{x}^{\alpha} - \mathbf{x}^{\beta}\right\|$, *i.e.*

$$\mathbf{f}^{\alpha} = -\sum_{\beta;\beta\neq\alpha} \frac{\partial\Phi(r_{\alpha\beta})}{\partial r_{\alpha\beta}} \tag{30}$$

For the nodal domain of influence in the coupling zone, only one element layer can be used in the continuum. This is necessary to avoid duplication of force computations.

On the region with no MD overlay, the internal forces can be calculated from

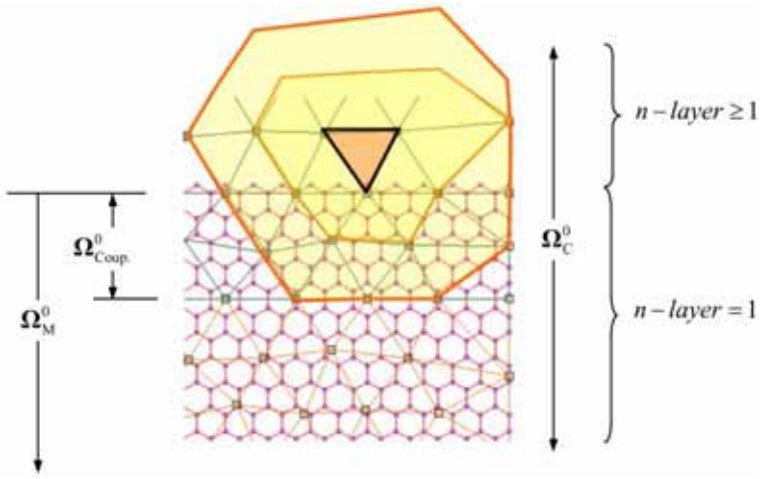

Fig. 7 The application of K-FEM in the proposed coupling method

$$\mathbf{F}^a_{\text{int}} = \sum_b \frac{\partial N^a(\mathbf{x}^b)}{\partial \mathbf{x}} \mathbf{P}_{\text{K}}(\mathbf{x}^b) w^b \tag{31}$$

where w^b is the quadrature weight corresponding to point $\mathbf{x}^b$ and $\mathbf{P}_{\text{K}}$ is the first Piola-Kirchoff stress defined as

$$\mathbf{P}_{\text{K}} = \frac{\partial W}{\partial F} \tag{32}$$

in which W and F denotes the potential energy density and the deformation gradient respectively. In this region, the nodal domain of influence can be expanded to more than one element layer based on the K-FEM concept as shown in Fig. 7.

3.2.3 Time integration over the coupling zone

In the coupling zone, the displacements of atoms and nodes are updated by using Eqs. (21) and (26) respectively. The corresponding accelerations can be obtained from

$$\ddot{\mathbf{u}}^{\alpha}_{\left(n+\frac{k+1}{m}\right)} = \frac{1}{\tilde{m}^{\alpha}}\left(\tilde{\mathbf{f}}^{\alpha}_{\text{ext}\left(n+\frac{k+1}{m}\right)} - \tilde{\mathbf{f}}^{\alpha}_{\text{int}\left(n+\frac{k+1}{m}\right)}\right) \tag{33}$$

and

$$\ddot{\mathbf{U}}^a_{(n+1)} = \frac{1}{\tilde{M}^a}(\tilde{\mathbf{F}}^a_{\text{ext}(n+1)} - \tilde{\mathbf{F}}^a_{\text{int}(n+1)}) \tag{34}$$

where

$$\tilde{m}^{\alpha} = w(\mathbf{x}^{\alpha}) m^{\alpha}; \tilde{M}^a = (1 - w(\mathbf{x}^a)) M^a \tag{35}$$

The internal and the external forces exerting on each atom of the molecular layer in the coupling zone should be factored by the scaling parameter as follows

$$\tilde{\mathbf{f}}_{\text{int}}^{\alpha} = w(\mathbf{x}^{\alpha})\mathbf{f}_{\text{int}}^{\alpha};\ \tilde{\mathbf{f}}_{\text{ext}}^{\alpha} = w(\mathbf{x}^{\alpha})\mathbf{f}_{\text{ext}}^{\alpha} \tag{36}$$

Similarly, the internal and the external forces acting on each node of the continuum layer in the coupling zone can be factored as

$$\tilde{\mathbf{F}}_{\text{int}}^{a} = (1 - w(\mathbf{x}^{a}))\mathbf{F}_{\text{int}}^{a};\ \tilde{\mathbf{F}}_{\text{ext}}^{a} = (1 - w(\mathbf{x}^{a}))\mathbf{F}_{\text{ext}}^{a} \tag{37}$$

After a typical micro step k, by adopting Eqs. (25) and (28), the unconstrained velocities of the atoms and nodes on the two sides of the coupling zone are given by

$$\dot{\hat{\mathbf{u}}}^{\alpha}_{\left(n+\frac{k+1}{m}\right)} = \dot{\mathbf{u}}^{\alpha}_{\left(n+\frac{k}{m}\right)} + \frac{1}{2}\left(\ddot{\mathbf{u}}^{\alpha}_{\left(n+\frac{k}{m}\right)} + \ddot{\mathbf{u}}^{\alpha}_{\left(n+\frac{k+1}{m}\right)}\right)\Delta t \tag{38}$$

$$\dot{\hat{\mathbf{U}}}^{a}_{\left(n+\frac{k+1}{m}\right)} = \dot{\mathbf{U}}^{a}_{\left(n+\frac{k}{m}\right)} + \frac{1}{2}(\ddot{\mathbf{U}}^{a}_{(n)} + \ddot{\mathbf{U}}^{a}_{(n+1)})\Delta t \tag{39}$$

For the continuum layer, while the nodal velocities are consistently updated after each of the m micro time steps, the nodal accelerations remain unchanged until a new global time station is reached.

The unconstrained velocities, Eqs. (38) and (39), must be further adjusted by applying the Lagrangian forces, Eqs. (19) and (20), as

$$\dot{\mathbf{u}}^{\alpha}_{\left(n+\frac{k+1}{m}\right)} = \dot{\mathbf{u}}^{\alpha}_{\left(n+\frac{k}{m}\right)} + \frac{1}{2}\left(\ddot{\mathbf{u}}^{\alpha}_{\left(n+\frac{k}{m}\right)} - \frac{1}{\tilde{m}^{\alpha}}\mathbf{f}^{\alpha}_{\lambda\left(n+\frac{k}{m}\right)} + \ddot{\mathbf{u}}^{\alpha}_{\left(n+\frac{k+1}{m}\right)} - \frac{1}{\tilde{m}^{\alpha}}\mathbf{f}^{\alpha}_{\lambda\left(n+\frac{k+1}{m}\right)}\right)\Delta t \tag{40}$$

$$\dot{\mathbf{U}}^{a}_{\left(n+\frac{k+1}{m}\right)} = \dot{\mathbf{U}}^{a}_{\left(n+\frac{k}{m}\right)} + \frac{1}{2}\left(\ddot{\mathbf{U}}^{a}_{(n)} - \frac{1}{\tilde{m}^{a}}\mathbf{F}^{a}_{\lambda\left(n+\frac{k}{m}\right)} + \ddot{\mathbf{U}}^{a}_{(n+1)} - \frac{1}{\tilde{m}^{a}}\mathbf{F}^{a}_{\lambda\left(n+\frac{k+1}{m}\right)}\right)\Delta t \tag{41}$$

By introducing $\boldsymbol{\lambda}^{\beta} = \frac{1}{2}\left(\boldsymbol{\lambda}^{\beta}_{\left(n+\frac{k}{m}\right)} + \boldsymbol{\lambda}^{\beta}_{\left(n+\frac{k+1}{m}\right)}\right)$ and utilizing the expression of the unconstrained velocities, the constrained velocities at the next micro time step can be updated as

$$\dot{\mathbf{u}}^{\alpha}_{\left(n+\frac{k+1}{m}\right)} = \dot{\hat{\mathbf{u}}}^{\alpha}_{\left(n+\frac{k+1}{m}\right)} + \frac{\Delta t}{\tilde{m}^{\alpha}}\sum_{\beta}^{n_{\lambda}}\boldsymbol{\lambda}^{\beta}\delta_{\alpha\beta} \tag{42}$$

$$\dot{\mathbf{U}}^{a}_{\left(n+\frac{k+1}{m}\right)} = \dot{\hat{\mathbf{U}}}^{a}_{\left(n+\frac{k+1}{m}\right)} - \frac{\Delta t}{\tilde{m}^{a}}\sum_{\beta}^{n_{\lambda}}\boldsymbol{\lambda}^{\beta}N^{a}(\mathbf{x}^{\beta}) \tag{43}$$

The Lagrange multipliers must be determined first in order to correct the unconstrained velocities according to Eqs. (42) and (43) by satisfying the velocity constraint of Eq. (18) in the following form

$$\dot{\mathbf{g}}^{\alpha}_{\left(n+\frac{k+1}{m}\right)} = \dot{\mathbf{U}}^{a}_{\left(n+\frac{k+1}{m}\right)}(\mathbf{x}^{a}) - \dot{\mathbf{u}}^{\alpha}_{\left(n+\frac{k+1}{m}\right)} = \sum_{a} N^{a}(\mathbf{x}^{\alpha})\dot{\mathbf{U}}^{a}_{\left(n+\frac{k+1}{m}\right)} - \dot{\mathbf{u}}^{\alpha}_{\left(n+\frac{k+1}{m}\right)} \tag{44}$$

Substituting Eqs. (42) and (43) into Eq. (44) yields the equation for solving the unknown Lagrange multipliers in the following form

$$\sum_{\beta}\mathbf{A}^{\alpha\beta}\boldsymbol{\lambda}^{\beta} = \hat{\mathbf{g}}^{\alpha} \tag{45}$$

where

$$\mathbf{A}^{\alpha\beta} = \Delta t\left(\frac{1}{\tilde{M}^a}\sum_a N^a(\mathbf{x}^\alpha)N^a(\mathbf{x}^\beta) + \frac{\delta_{\alpha\beta}}{\tilde{m}^\alpha}\right) \tag{46}$$

and

$$\hat{\mathbf{g}}^\alpha = \sum_a N^a(\mathbf{x}^\alpha)\ \dot{\hat{\mathbf{U}}}^a - \dot{\hat{\mathbf{u}}}^\alpha \tag{47}$$

In order to reduce the computational cost, the constraint matrix, $\mathbf{A}^{\alpha\beta}$, can be simplified to a diagonal $n \times n$ matrix in which $n = n_{\mathrm{SD}} \times n_\lambda$. The diagonalized matrix is then expressed as

$$\mathbf{A}^{\alpha\alpha} = \Delta t\sum_\beta\left(\frac{1}{\tilde{M}^a}\sum_a N^a(\mathbf{x}^\alpha)N^a(\mathbf{x}^\beta) + \frac{\delta_{\alpha\beta}}{\tilde{m}^\alpha}\right) \tag{48}$$

The resulting unknown Lagrange multipliers can be obtained by

$$\boldsymbol{\lambda}^\alpha = \mathbf{A}^{\alpha\alpha-1}\hat{\mathbf{g}}^\alpha \tag{49}$$

4. Numerical examples

Dynamic wave propagation in 1D atomic lattice is chosen to illustrate the validity and the effectiveness of the proposed multiscale coupling method. This similar example was tested by Wagner and Liu (2003) and Park and Liu (2004). In this problem, the Lennard-Jones (LJ) 6-12 interatomic potential is used to simulate force between the atoms as expressed by

$$\Phi_{\mathrm{LJ}}(r_{\alpha\beta}) = 4\bar{\Phi}\left(\frac{\bar{r}^{12}}{r_{\alpha\beta}^{12}} - \frac{\bar{r}^6}{r_{\alpha\beta}^6}\right) \tag{50}$$

where $\bar{\Phi}$ is the depth of the potential energy well, $r_{\alpha\beta}$ is the pair-wise distance between the atoms and $\bar{r}$ is the value of r at which the potential energy becomes zeros. The LJ 6-12 potential and its corresponding interatomic force are plotted versus the interatomic distance in Fig. 8, using the dimensionless quantities (Liu *et al.* 2006). From Fig. 8, the equilibrium distance, r_0, can be obtained as

$$r_0 = \sqrt[6]{2}\bar{r} \tag{51}$$

For simplicity, the mass of atom, $\bar{\Phi}$ and $\bar{r}$ parameters are assumed to be a unity in this study. As a result, the equilibrium bond length, r_0, is reduced to $\sqrt[6]{2}\bar{r} = 1.1225$ and the LJ 6-12 expression in Eq. (50) can be rewritten as

$$\Phi_{\mathrm{LJ}}(r_{\alpha\beta}) = 4\left(\frac{1}{r_{\alpha\beta}^{12}} - \frac{1}{r_{\alpha\beta}^6}\right) \tag{52}$$

The corresponding atomic force on atom α can be evaluated using Eq. (30) as

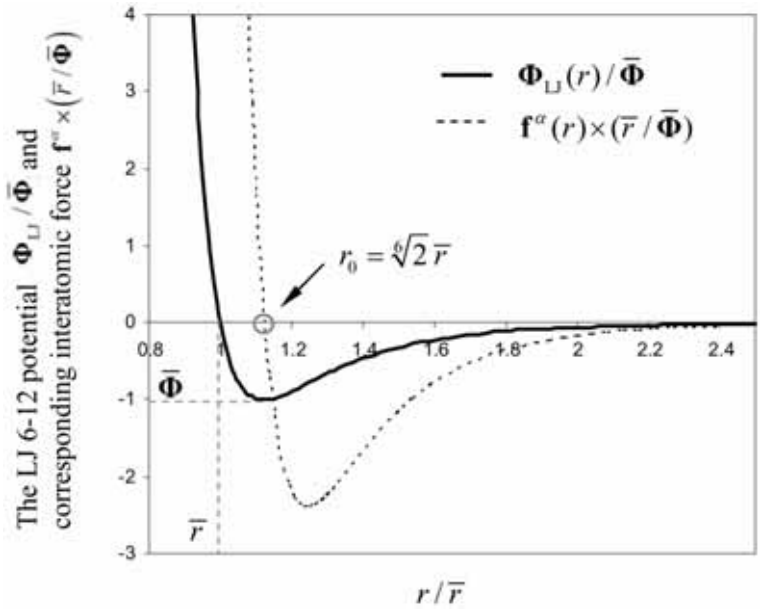

Fig. 8 Lennard-Jones (LJ 6-12) potential and its corresponding interatomic force

$$\mathbf{f}^{\alpha} = -\sum_{\beta;\beta\neq\alpha}\frac{\partial\Phi(r_{\alpha\beta})}{\partial r_{\alpha\beta}} = -24\sum_{\beta;\beta\neq\alpha}\left(\frac{1}{r_{\alpha\beta}^{7}}-\frac{2}{r_{\alpha\beta}^{13}}\right) \tag{53}$$

Based on Eq. (32), the first Piola-Kirchoff stress $\mathbf{P}_{\mathrm{K}}$ can be obtained as

$$\mathbf{P}_{\mathrm{K}} = \frac{\partial W}{\partial F} = \left(\frac{24}{F^{7}r_0^{7}}-\frac{48}{F^{13}r_0^{13}}\right) = \left(\frac{24}{r^{7}}-\frac{48}{r_0^{13}}\right) \tag{54}$$

where $r = Fr_0$.

The initial displacement of an atom as a result of a Gaussian pulse can be given as

$$u(\mathbf{x},t=0) = \begin{cases} A\left(\dfrac{e^{-(\mathbf{x}/\zeta)^2}-e^{-(\mathbf{x}_s/\zeta)^2}}{1-e^{-(\mathbf{x}_s/\zeta)^2}}\right)\left(1+b\cos\left(\dfrac{2\pi\mathbf{x}}{H}\right)\right) & \text{if } |\mathbf{x}|\le\mathbf{x}_s \\ 0 & \text{if } |\mathbf{x}|>\mathbf{x}_s \end{cases} \tag{55}$$

in which $A = 0.015$, $b = 0.2$, $\zeta = 20$, $H = (\zeta/4)$ and $\mathbf{x}_s = 5\zeta$.

Since this problem is symmetric about $x = 0$, only the initial condition in $+x$ plane is plotted in Fig. 9. It can be observed from the initial condition that a spectrum of waves from low to high frequencies occur in the MD layer. The K-FEM of forty equally distributed nodes is used over the domain where $-200r_0 \le x \le 200r_0$. The MD simulation is performed in the subdomain of $-60r_0 \le x \le 60r_0$ with totally 121 atoms being distributed uniformly. As a result, the nodal spacing in the continuum model is 10 times that of the atomic spacing.

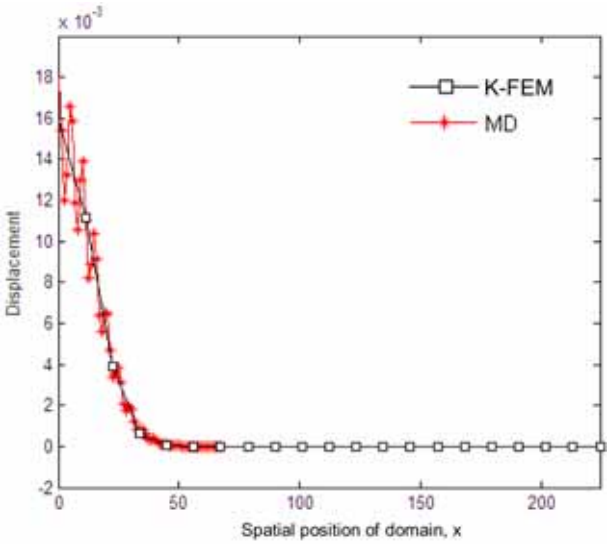

Fig. 9 Initial displacements prescribed by a Gaussian pulse

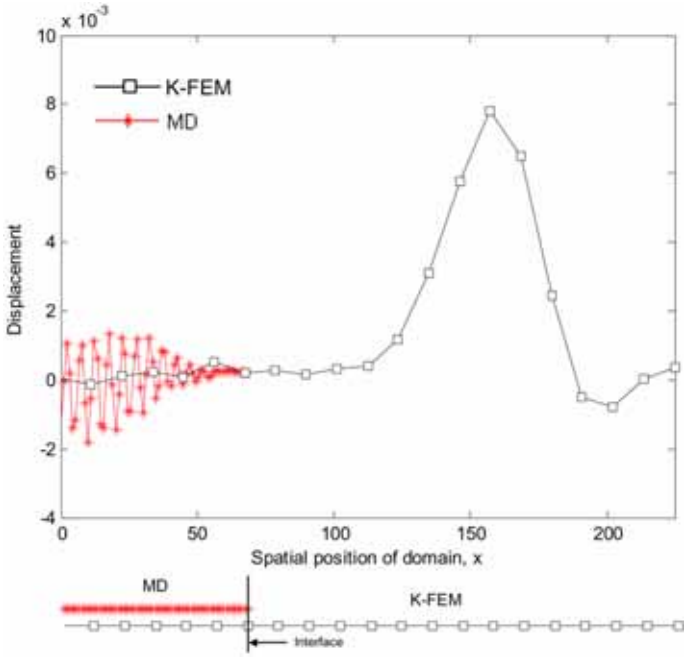

Fig. 10 Illustration of spurious wave reflection at MD/K-FEM interface without enforcement of displacement compatibility

This study attempted to investigate the following effects: (1) the size of the coupling zone and (2) the size of the K-FEM nodal domain of influence. In this test, the global time step, ΔT, is 0.35 while the micro time step, $\Delta t = \Delta T / 50$.

For comparison purpose, the same problem is also analyzed without displacement compatibility

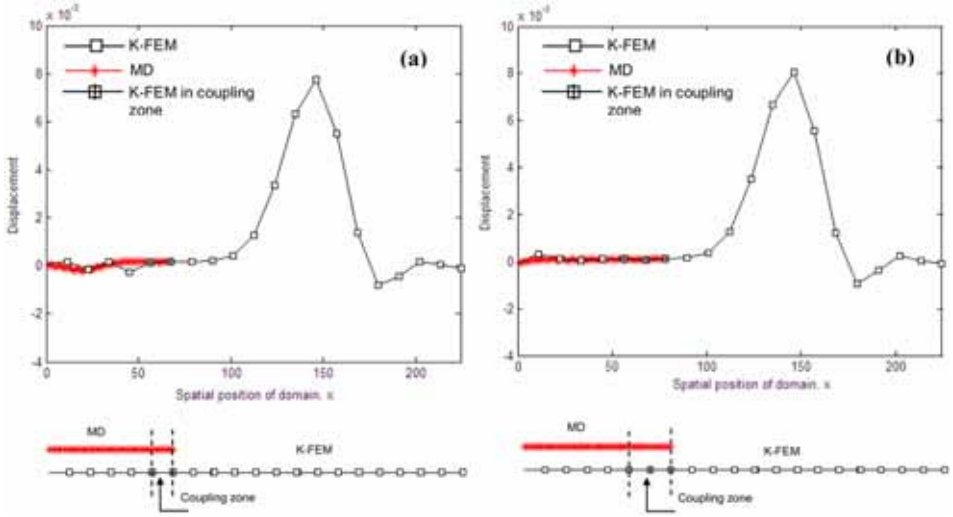

Fig. 11 Displacement profile obtained by the present method using (a) one element over 11 atoms and (b) two elements over 21 atoms at the coupling zone

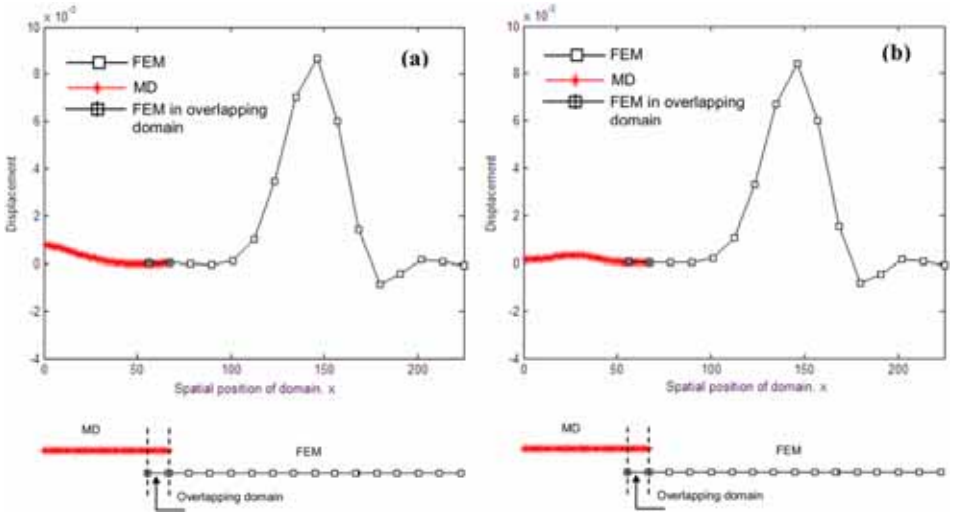

Fig. 12 Results of displacement of the same problem obtained by the BDM (Xiao and Belytschko 2004) with (a) linear and (b) non-linear scaling parameters

condition. As can be seen in Fig. 10, the spurious wave reflection was observed in the molecular domain at the MD/K-FEM interface when the two models are coupled with no treatment of displacement compatibility. However by the present method with enforcement of displacement compatibility, the snapshot of the displacement time history at time $t = 16.45$ was shown in Fig. 11, one using a coupling zone of 1 element over 11 atoms and the other 2 elements over 21 atoms. The spurious wave reflection is almost completely eliminated in the present method.

To investigate the effectiveness of the present method, the same problem was also tested by the BDM (Xiao and Belytschko 2004) using linear and non-linear scaling parameters. In the BDM, the

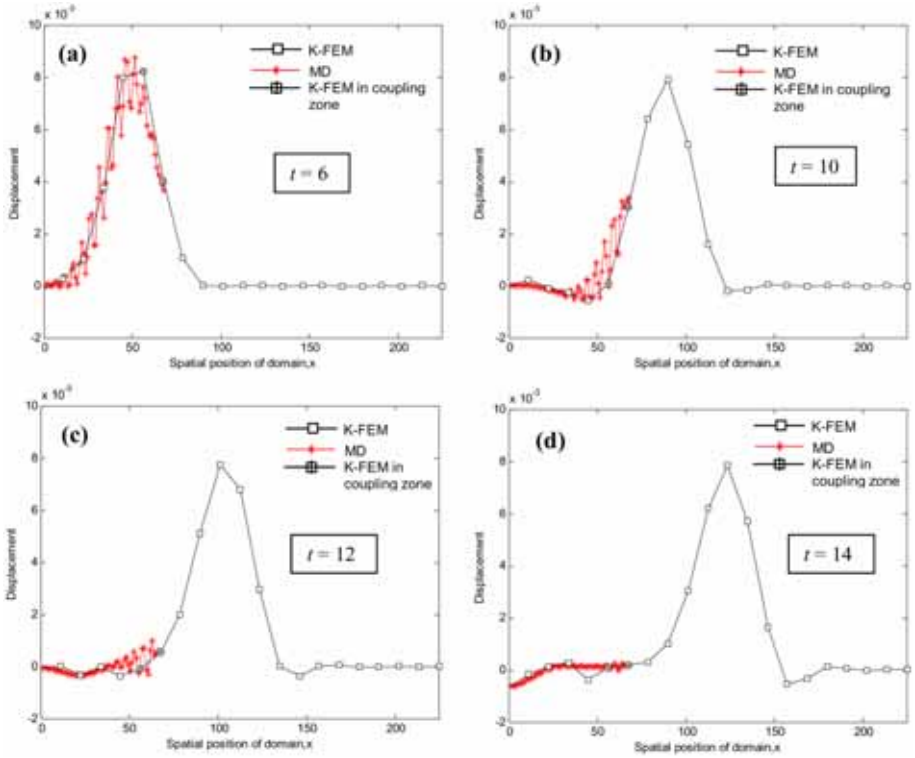

Fig. 13 Displacement profiles by present method at different moments

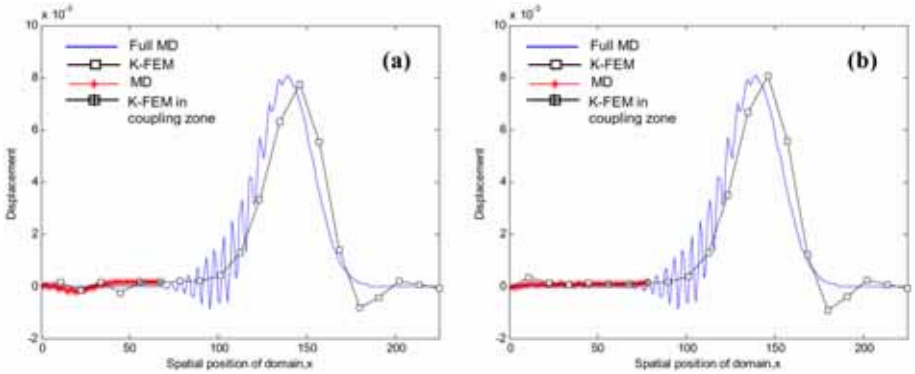

Fig. 14 Comparison of displacement profiles computed by a full MD simulation and the proposed method with (a) one and (b) two elements coupling

continuum model does not cover the entire domain like the present method. Their results for this problem are displayed in Fig. 12. By comparing with Fig. 11(a), it can be found that by applying K-FEM over the entire domain and using quartic spline scaling parameter in the coupling zone, the present method provides a better seamless transition across different length scales.

The displacement profiles at various times obtained by the present method using a coupling zone of one element are plotted in Fig. 13. At time $t = 6$, the first wave front has started to attack the

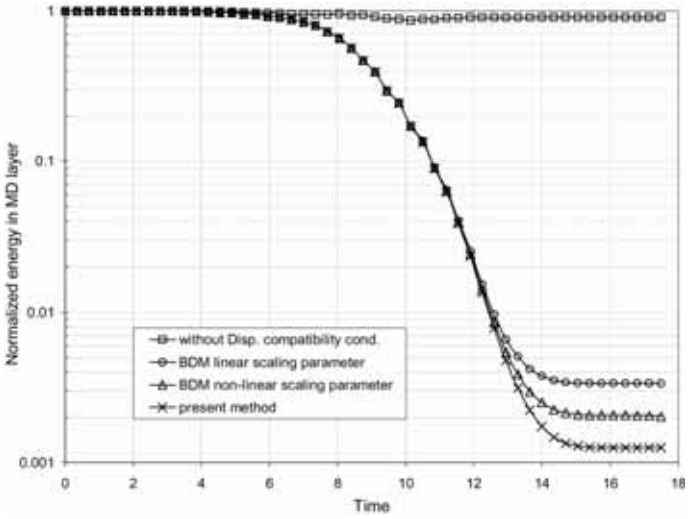

Fig. 15 Time history showing energy residual in the MD layer after transfer

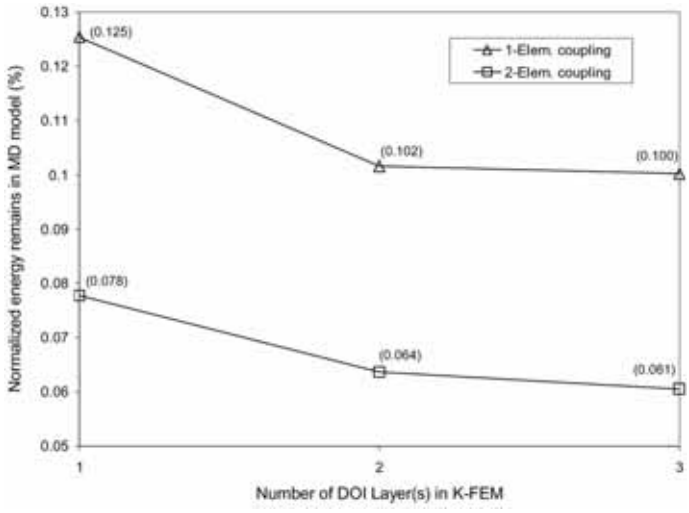

Fig. 16 Comparison of residual energy in MD with 1-3 element layers of nodal domain of influence in K-FEM for 1 and 2 element coupling zone

coupling zone and the spurious wave reflection in MD layer is not observed. At the transient state, as depicted in subplots (b) and (c), the wave has propagated across the coupling zone and the reflections are noticeable in the MD layer. At time $t = 14$, the wave has completely passed the coupling zone. It can also be observed that only a small amount of energy is trapped in the MD layer. Furthermore, the displacement profiles at the steady state obtained by the present method and a full MD simulation are compared in Fig. 14. As can be seen, the essential characteristics of Gaussian wave can be captured by either a one-element or a two-element coupling in the present method.

For clarity, the time history of the total energy, normalized by its initial value in the MD layer is

plotted in Fig. 15 for each of the four cases. It is clear that the present method is most effective in transferring energy from the MD layer to the continuum base layer. Using one element overlaying 11 atoms in the present method, only 0.125% of the total energy was trapped in the MD layer while 0.338% and 0.207% of the total energy were trapped in the two cases of BDM using linear and nonlinear scaling parameters respectively.

The effect of extending NDOI from the conventional 1 to 2 and 3 layers of elements, referred as *l*-refinement (Kanok-Nukulchai and Wong 2008), is also investigated. It can be concluded that *l*-refinement can further improve the energy transfer of the interface as seen in Fig. 16. For 1 element coupling zone, increasing NDOI from 1 to 2 and 3 layers serves to reduce the trapped total energy from 0.125% to 0.102% and 0.100% respectively. Similar trend was also observed in the case of 2 elements coupling zone, where the trapped total energy can be reduced from 0.078% to 0.064% and 0.061% using the *l*-refinement.

5. Conclusions

A concurrent multiscale simulation for coupling two models of different scales, *i.e.*, the molecular and the continuum dynamics, has been presented and validated. In the proposed method, the K-FEM is employed to model the entire domain in coexistence with the MD simulation over a specific localized region of interest. The coupling between the continuum and the molecular models is achieved by using a quartic spline scaling parameter to integrate their Hamiltonians. The displacement compatibility condition over the coupling zone is imposed by the Lagrange multipliers technique. In addition, a multiple-time-step velocity Verlet algorithm is employed to perform their intrinsic time integrations.

The effectiveness of the proposed method is confirmed by solving non-linear problems in 1D atomic lattice with Lennard-Jones (LJ) 6-12 potential. The numerical results reveal that the proposed coupling method can efficiently eliminate the spurious wave reflection at the molecular/continuum interface. As a result, the energy in the MD model can be almost completely transferred into the continuum domain.

The efficiency of the proposed coupling methodology can be greatly enhanced by either increasing the size of the coupling zone or extending the nodal domain of influence over more element layers around the node based on K-FEM. Furthermore, by allowing MD to overlay on a specific area of K-FEM domain, MD force can be extrapolated to yield the corresponding internal force in the continuum layer. This will ensure the seamless transition between the two different length scales.

In summary, there are two major advantages of the present method. First, it does not require any filtering or damping function to eliminate the spurious wave reflection. Secondly, it does not require the continuum mesh to grade down to the atomic spacing in the coupling zone. Thus, the method provides a sound basis for further extending to more complicated problems involving atomic structure, and can be straightforwardly extended to two- and three-dimensional multiscale problems.

Acknowledgements

This study is a part of the doctoral dissertation of the first author. The supports of the Royal Thai

Government, the Government of Austria, Asian Institute of Technology and Ubon Ratchathani Rajabhat University are gratefully acknowledged. The authors also would like to recognize the cooperation of the Computational Nanoscience Consortium (CNC), Thailand.

References

Abraham, F., Broughton, J., Bernstein, N. and Kaxiras, E. (1998), "*Spanning the continuum to quantum length scales in a dynamic simulation of brittle fracture*", *EPL-Europhys. Lett*., **44**, 783-787.

Adelman, S.A. and Doll, J.D. (1976), "Generalized langevin theory for atom/solid-surface scattering: General formulation for classical scattering off harmonic solids", *J. Chem. Phys.*, **64**, 2375-2388.

Arroyo, M. and Belytschko, T. (2002), "An atomistic-based finite deformation membrane for single layer crystalline films", *J. Mech. Phys. Solids*, **50**, 1941-1977.

Arroyo, M. and Belytschko, T. (2003), "A finite deformation membrane based on inter-atomic potentials for the transverse mechanics of nanotubes", *Mech. Mater.*, **35**, 193-215.

Arroyo, M. and Belytschko, T. (2004), "Finite element methods for the non-linear mechanics of crystalline sheets and nanotubes", *Int. J. Numer. Meth. Eng.*, **59**, 419-456.

Belytschko, T., Lu, Y.Y. and Gu, L. (1994), "Element-free Galerkin methods", *Int. J. Numer. Meth. Eng.*, **37**, 229-256.

Belytschko, T. and Xiao, S.P. (2003), "Coupling methods for continuum model with molecular model", *Int. J. Multiscale Com.*, **1**, 115-126.

Cressie, N. A. (1993), *Statistics for Spatial data*, Wiley, New York.

Dai, K.Y., Liu, G.R., Lim, K.M. and Gu, Y.T. (2003), "Comparison between the radial point interpolation and the Kriging interpolation used in meshfree methods", *Comput. Mech.*, **32**, 60-70.

Dolbow, J. and Belytschko, T. (1998), "An Introduction to Programming the Meshless Element Free Galerkin Method", *Comp. Mech. Eng.*, **5**, 207-241.

Gu, L. (2003), "Moving Kriging interpolation and element-free Galerkin method", *Int. J. Numer. Meth. Eng.*, **56**, 1-11.

Kanok-Nukulchai, W. and Plengkhom, K. (2004), "An extended FEM with element-free shape functions", *Abstract presented at WCCM VI in conjunction with APCOM'04*, Beijing, China.

Kanok-Nukulchai, W., Plengkhom, K. and Tongsuk, P. (2004), "Element-free shape functions for superior performance of FEM", *Abstract presented at IWACOM*, Tokyo, Japan.

Kanok-Nukulchai, W. and Wong, F.T. (2008). "A break-through enhancement of FEM using node-based Kriging interpolation", *Bull. Int. Assoc. Comp. Mech*., **23**, 26-31.

Liu, W.K., Karpov, E.G. and Park, H.S. (2006), *Nano mechanics and materials: theory, multiscale methods and applications*, John Wiley & Sons Ltd, England.

Liu, W.K., Karpov, E.G., Zhang, S. and Park, H.S. (2004), "An introduction to computational nano mechanics and materials", *Comput. Method. Appl. M.*, **193**, 1529-1578.

Park, H.S. and Liu, W.K. (2004), "Introduction and tutorial on multiple scale analysis in solids", *Comput. Method. Appl. M*., **193**, 1733-1772.

Park, H.S., Kapov, E.G., Liu, W.K. and Klein, P.A. (2005a), "The bridging scale for two-dimensional atomistic/ continuum coupling", *Philos. Mag*., **85**, 79-113.

Park, H.S., Karpov, E.G., Klein, P.A. and Liu, W.K. (2005b), "Three-dimensional bridging scale analysis of dynamic fracture", *J. Comput. Phys.*, **207**, 588- 609.

Plengkhom, P. and Kanok-Nukulchai, W. (2005), "An enhancement of finite element method with moving Kriging shape functions", *Int. J. Comput. Meth.*, **2**, 451-475.

Qian, D. and Gondhalekar, R.H. (2004), "A virtual atom cluster approach to the mechanics of nanostructures", *Int. J. Multiscale. Com.*, **2**, 227-289.

Rudd, R.E. and Broughton, J.Q. (1998), "Coarse-grained molecular dynamics and the atomic limit of finite element", *Phys. Rev. B.*, **58**, 5893-5896.

Sommanawat, W. and Kanok-Nukulchai, W. (2008), "Multiscale simulation based on Moving Kriging method",

Abstract presented at WCCM8 and ECCOMAS 2008, Venice, June - July.
Tadmor, E., Ortiz, M. and Phillips, R. (1996), "Quasicontinuum analysis of defects in solids", *Philos. Mag. A.*, **73**, 1529-1563.
Tang, S., Hou, T.Y. and Liu, W.K. (2006), "A mathematical framework of the bridging scale method", *Int. J. Numer. Meth. Eng.*, **65**, 1688-1713.
Tongsuk, P. and Kanok-Nukulchai, W. (2004), "Further investigation of element-free Galerkin method using moving Kriging interpolation", *Int. J. Comput. Meth.*, **1**, 345-365.
Xiao, S.P. and Belytschko, T. (2004), "A bridging domain method for coupling continua with molecular dynamics", *Comput. Method. Appl. M.*, **193**, 1645-1699.
Xu, M. and Belytschko, T. (2008), "Conservation properties of the bridging domain method for coupled molecular/continuum dynamics", *Int. J. Numer. Meth. Eng.*, **76**, 278-294.
Wagner, G.J. and Liu, W.K. (2003), "Coupling of atomistic and continuum simulations using a bridging scale decomposition", *J. Comput. Phys.*, **190**, 249-274.
Wong, F.T. and Kanok-Nukulchai, W. (2009), "On the convergence of the Kriging based finite element method", *Int. J. Comput. Meth.*, **6**, 93-118.
Zhang, S., Khare, R., Lu, Q. and Belytschko, T. (2007), "A bridging domain and strain computation method for coupled atomistic-continuum modeling of solids", *Int. J. Numer. Meth. Eng.*, **70**, 913-933.